95.4 GeV diphoton excess at ATLAS and CMS

Thomas Biekötter,[1,*] Sven Heinemeyer,[2,†] and Georg Weiglein[3,4,‡]
[1]*Institute for Theoretical Physics, Karlsruhe Institute of Technology, Wolfgang-Gaede-Straße 1, 76131 Karlsruhe, Germany*
[2]*Instituto de Física Teórica UAM-CSIC, Cantoblanco, 28049, Madrid, Spain*
[3]*Deutsches Elektronen-Synchrotron DESY, Notkestrße 85, 22607 Hamburg, Germany*
[4]*II. Institut für Theoretische Physik, Universität Hamburg, Luruper Chaussee 149, 22761 Hamburg, Germany*

(Received 29 July 2023; accepted 18 January 2024; published 8 February 2024)

The ATLAS Collaboration has recently reported the results of a low-mass Higgs-boson search in the diphoton final state based on the full Run 2 dataset. The results are based on an improved analysis with respect to the previous analysis, which included a part of the Run 2 data, with a substantially better sensitivity. The "model-dependent" search carried out by ATLAS shows an excess of events at a mass of about 95.4 GeV with a local significance of 1.7σ. The results are compatible with a previously reported excess at the same mass, but with somewhat higher significance of 2.9σ, from the CMS collaboration, also based on the full Run 2 dataset. Combining the two results (neglecting possible correlations), we find a signal strength of $\mu_{\gamma\gamma}^{\mathrm{ATLAS+CMS}} = 0.24^{+0.09}_{-0.08}$, corresponding to an excess of 3.1σ. In this work, we investigate the implications of this result, updating a previous analysis based solely on the CMS Run 2 data. We demonstrate that the ATLAS/CMS combined diphoton excess can be interpreted as the lightest Higgs boson in a Two-Higgs doublet model that is extended by a complex singlet (S2HDM) of Yukawa types II and IV, while being in agreement with all other experimental and theoretical constraints.

DOI: 10.1103/PhysRevD.109.035005

I. INTRODUCTION

More than a decade after the discovery of a Higgs boson with a mass of about 125 GeV by the ATLAS and CMS Collaborations [1,2], the search for additional Higgs bosons continues to be one of the prime tasks of the LHC physics program. Searches for Higgs bosons below 125 GeV have been performed at LEP [3–5], the Tevatron [6], and the LHC [7–14]. Among them, CMS has performed searches for scalar diphoton resonances at 8 TeV and 13 TeV. Results based on the 8 TeV data and the full Run 2 dataset at 13 TeV showed a local excess of 2.9σ at 95.4 GeV [13]. This excess, which is present in both the 8 TeV and the 13 TeV dataset, received considerable attention already soon after it was made public using the first year of Run 2 data; see, e.g., Refs. [15–25]. Analyses using the result based on the full Run 2 data can be found in Refs. [26,27] (see also Ref. [28]).

Recently, ATLAS presented the result based on their full Run 2 dataset [14,29]. In the following, we refer to the "model-dependent" analysis from ATLAS, which has a higher discriminating power. The new analysis has a substantially improved sensitivity with respect to their analysis based on the previously reported result utilizing 80 fb^{-1} [10]. ATLAS finds an excess with a local significance of 1.7σ at precisely the same mass value as the one that was previously reported by CMS, namely at 95.4 GeV. This "diphoton excess" can be described by a scalar resonance at 95.4 GeV with a signal strength of

$$\mu_{\gamma\gamma}^{\mathrm{ATLAS}} = \frac{\sigma^{\mathrm{exp}}(pp \to \phi \to \gamma\gamma)}{\sigma^{\mathrm{SM}}(pp \to H \to \gamma\gamma)} = 0.18^{+0.10}_{-0.10}, \qquad (1)$$

which we determined based on the reported expected and observed limits at 95.4 GeV and the reported significance of the excess. Here, σ^{SM} denotes the cross section for a hypothetical SM Higgs boson at the same mass. Since ATLAS presented their results as limits on the total cross section, we normalized these limits with the SM prediction $\sigma^{\mathrm{SM}}(pp \to H \to \gamma\gamma) = 126$ pb [30] in order to find the value for $\mu_{\gamma\gamma}^{\mathrm{ATLAS}}$ shown in Eq. (1). The corresponding CMS result for a mass of 95.4 GeV is given by [13]

*thomas.biekoetter@kit.edu
†sven.heinemeyer@cern.ch
‡georg.weiglein@desy.de

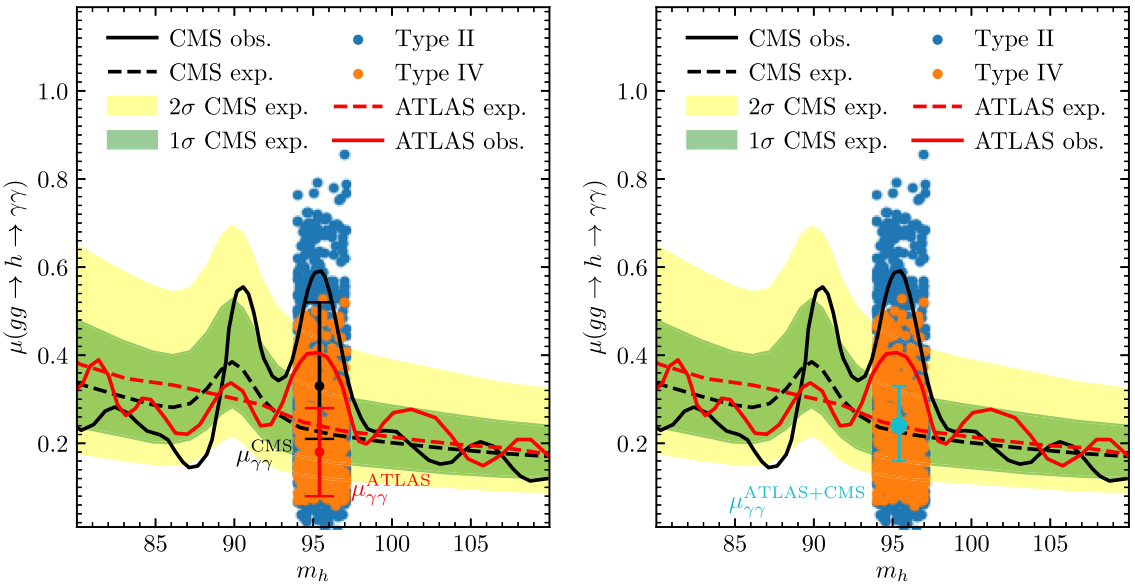

FIG. 1. S2HDM parameter points passing the applied constraints in the $(m_{h_1}, \mu_{\gamma\gamma})$ plane for the type II (blue) and the type IV (orange). The expected and observed cross section limits obtained by CMS are indicated by the black dashed and solid lines, respectively, and the 1σ and 2σ uncertainty intervals are indicated by the green and yellow bands, respectively. Overlaid in red are the expected and observed limits from ATLAS [14]. The values of $\mu_{\gamma\gamma}^{\mathrm{ATLAS}}$, $\mu_{\gamma\gamma}^{\mathrm{CMS}}$, and $\mu_{\gamma\gamma}^{\mathrm{ATLAS+CMS}}$ and their respective uncertainties are indicated by the red, black (left plot), and cyan (right plot) error bars at 95.4 GeV.

$$\mu_{\gamma\gamma}^{\mathrm{CMS}} = \frac{\sigma^{\mathrm{exp}}(pp \to \phi \to \gamma\gamma)}{\sigma^{\mathrm{SM}}(pp \to H \to \gamma\gamma)} = 0.33^{+0.19}_{-0.12}. \tag{2}$$

Regarding the interpretation of the new result from ATLAS together with the previously reported one from CMS, it is important to note that a possible signal at about 95 GeV giving rise to a relatively small number of events would occur on top of a much larger fluctuating background. Therefore, one cannot necessarily expect that the excesses should occur with exactly the same signal strength, and the fact that both collaborations report their most significant excess at precisely the same mass value has to be seen in this context as a certain level of coincidence. Since for the same mass value, the signals strengths $\mu_{\gamma\gamma}^{\mathrm{ATLAS}}$ and $\mu_{\gamma\gamma}^{\mathrm{CMS}}$ agree with each other within their uncertainties, we regard the two results to be compatible with each other. It should also be noted in this context, see Fig. 1 below, that the upper bound observed by ATLAS at 95.4 GeV, albeit slightly stronger than the one observed by CMS at this mass value, lies significantly above the signal interpretation of the CMS result that is reflected in $\mu_{\gamma\gamma}^{\mathrm{CMS}}$. Neglecting possible correlations, we obtain a combined signal strength of

$$\mu_{\gamma\gamma}^{\mathrm{exp}} = \mu_{\gamma\gamma}^{\mathrm{ATLAS+CMS}} = 0.24^{+0.09}_{-0.08}, \tag{3}$$

corresponding to an excess of 3.1σ at

$$m_\phi \equiv m_\phi^{\mathrm{ATLAS+CMS}} = 95.4\ \mathrm{GeV}. \tag{4}$$

If the origin of the diphoton excesses at 95.4 GeV is a new particle, which is the scenario that we investigate here, the question arises whether it is also detectable in other collider channels. In addition, the new particle could have been produced already in small numbers in other existing searches. In this regard, it is interesting to note that LEP reported a local 2.3σ excess in the $e^+e^- \to Z(\phi \to b\bar{b})$ searches [4], which would be consistent with a scalar resonance with a mass of about 95.4 GeV and a signal strength of $\mu_{bb}^{\mathrm{exp}} = 0.117 \pm 0.057$ [15,31]. In addition to the diphoton excess, CMS observed another excess compatible with a mass of 95.4 GeV in the Higgs-boson searches utilizing di-tau final states [11]. This excess was most pronounced at a mass of 100 GeV with a local significance of 3.1σ, but it is also well compatible with a mass of 95.4 GeV, where the local significance amounts to 2.6σ, and where the corresponding signal strength for a mass hypothesis of 95 GeV was determined to be $\mu_{\tau\tau}^{\mathrm{exp}} = 1.2 \pm 0.5$. ATLAS has not yet published a search in the di-tau final state that covers the mass range around 95 GeV.

Given that all the excesses discussed above occurred at a similar mass, it is possible that they arise from the production of a single new particle, which would be a first sign of physics beyond the SM (BSM) in the Higgs-boson sector. This triggered activities in the literature regarding possible model interpretations that could account for the various excesses [15–27,32–37]. The first analysis using

the CMS result based on the full Run 2 data can be found in Ref. [26].

Since the new result from ATLAS implies that a moderate diphoton excess at about 95 GeV has independently been observed by two different experiments, it is of interest to assess the implications of the combined result from ATLAS and CMS on possible model interpretations. In the present paper, we focus in particular on the extension of the 2HDM by a complex singlet (S2HDM) as a template for a model where a mostly gauge-singlet scalar particle obtains its couplings to fermions and gauge bosons via the mixing with the SM-like Higgs boson at 125 GeV. We will demonstrate that this kind of scenario is suitable for describing the diphoton excess, taking into account the (in comparison to the CMS result slightly increased) significance of the combined result. Moreover, we will discuss the possibility of simultaneously describing the $b\bar{b}$ excess and the di-tau excess.

The paper is structured as follows. In Sec. II A, we briefly introduce the S2HDM and define our notation. In Sec. II B, we provide a brief qualitative discussion on how sizable signal rates in the three channels in which the excesses have been observed can arise. The relevant theoretical and experimental constraints on the model parameters are briefly summarized in Sec. II C. We present our main results regarding the numerical analysis of the improved significance of the diphoton excess in Sec. III. The conclusions and an outlook are given in Sec. IV.

II. A 95 GeV HIGGS BOSON IN THE S2HDM

In this section, we briefly summarize the scalar sector of S2HDM and how the excesses at about 95 GeV can be accommodated in this model. We also review the relevant experimental and theoretical constraints that are applied in our numerical analysis.

A. Model definitions

The S2HDM extends the SM, containing only one SU(2) Higgs doublet Φ_1, by a second Higgs doublet field Φ_2 and an additional complex gauge-singlet field Φ_S [32,38]. As in the 2HDM, in the S2HDM, the electroweak symmery is spontaneously broken by the two vacuum expectation values (vevs) of the two Higgs doubles, v_1 and v_2, with $\tan\beta = v_2/v_1$, and $v_1^2 + v_2^2 = v^2 \approx (246\ \text{GeV})^2$ corresponds to the SM vev squared. In addition, the real component of the singlet field has the nonzero vev v_S. Imposing a softly broken U(1) symmetry under which only Φ_S is charged, the imaginary part of the singlet gives rise to the presence of a stable pseudo-Nambu-Goldstone DM state. This yields the attractive possibility of accommodating the observed DM relic abundance via the usual freeze-out mechanism. Neglecting possible sources of CP violation, as we do throughout this paper for simplicity, the physical scalar spectrum of the S2HDM consists of three CP-even Higgs bosons $h_{1,2,3}$ with masses $m_{h_{1,2,3}}$, a pair of charged Higgs bosons $H^\pm$, and a CP-odd Higgs boson A with masses $m_{H^\pm}$ and m_A, respectively, as well as a stable scalar DM candidate χ.

We impose an additional Z_2 symmetry under which one of the doublet fields changes the sign in order to avoid flavor changing neutral currents at the tree level. The Z_2 symmetry is only softly broken via a term of the form $-m_{12}^2(\Phi_1^\dagger\Phi_2 + \text{H.c.})$. This symmetry implies for the fermion sector that either Φ_1 or Φ_2 (but not both) couples to either the charged leptons ℓ, the up-type quarks u or the down-type quarks d, leading to the four Yukawa types of the model [39]: type I, II, III (lepton specific), and IV (flipped).

B. Interpretation of the excesses

In the following discussion, the lightest of the three CP-even Higgs bosons of the S2HDM h_1 serves as the possible particle state at about 95 GeV, also denoted h_{95} from here on. We furthermore assume that the second lightest Higgs boson, $h_2 = h_{125}$, corresponds to the state discovered at about 125 GeV. The key aspect of the signal interpretation presented here is that h_{95} obtains its couplings to the fermions and gauge bosons as a result of the mixing with the CP-even components of the two doublets. Despite the predominantly singletlike character of h_{95}, sizable decay rates into diphoton pairs can be achieved via a suppression of the otherwise dominating decay into b-quark pairs (see also Ref. [40]). At the same time, no such suppression should occur for the coupling to top quarks, whose loop contribution gives rise to the decay into photons and also governs the production process via gluon fusion. In the Yukawa types II and IV, Φ_1 is coupled to down-type quarks, and Φ_2 is coupled to up-type quarks. In this case, an independent modification of the couplings of the Higgs bosons h_i to bottom quarks and top quarks is possible. These two types are therefore of particular interest regarding the prediction of a sufficiently large diphoton signal rate (see Ref. [26] for a detailed discussion). On the other hand, between these two types, an important difference arises from the fact that $c_{h_{95}\tau^+\tau^-}$ is equal to $c_{h_{95}b\bar{b}}$ in type II, while it is equal to $c_{h_{95}t\bar{t}}$ in type IV. Accordingly, in type II, no sizable signal rates in the $\tau^+\tau^-$ decay channel can be achieved if the diphoton excess is accommodated, whereas in type IV, a larger rate in the $\tau^+\tau^-$ channel can occur simultaneously with a relatively large rate in the $\gamma\gamma$ channel [35].

C. Constraints

The parameter space that is relevant for a possible description of the excesses at about 95 GeV is subject to various theoretical and experimental constraints.

Theoretical constraints that we apply in our analysis ensure that the perturbative treatment of the scalar sector

of the S2HDM is valid by demanding agreement with perturbative unitarity constraints [32]. In addition, according to the approach described in Ref. [32], we require that the tree-level scalar potential is bounded from below and that the electroweak vacuum corresponds to the global minimum of the potential.

With regard to the experimental constraints, we check whether the parameter points are in agreement with the cross section limits from BSM Higgs searches by making use of the public code HiggsBounds [41–45] (as part of the new code HiggsTools v.1 [45]). A parameter point is rejected if the signal rate of one of the Higgs bosons in the most sensitive search channel (based on the expected limits) is larger than the experimentally observed limit at the 95% confidence level. In order to ensure that the properties of h_{125} are in agreement with the measured signal rates from the LHC, we make use of the public code HiggsSignals [45–48] (also part of HiggsTools [45]). We regard a parameter point as accepted for $\chi^2_{125} \leq \chi^2_{\mathrm{SM},125} + 6.18$, where χ^2_{125} is the value of a χ^2 fit to the various LHC cross-section measurements in the S2HDM, and $\chi^2_{\mathrm{SM},125}$ is the SM fit result. In two-dimensional parameter estimations, in which other free parameters are profiled over, the above condition ensures that the accepted S2HDM parameter points are not disfavored by more than 2σ in comparison to the SM from the LHC rate measurements.

Flavor-physics observables and from electroweak precision observables give rise to indirect experimental constraints on the Higg sector of the S2HDM. We apply lower limits of $\tan\beta > 1.5$ and $m_{H^\pm} > 600$ GeV in our S2HDM parameter scans in type II and type IV to ensure agreement with the flavor-physics constraints [49]. Regarding electroweak precision observabes, we apply constraints in terms of the oblique parameters S, T, and U, computed according to Ref. [50] at the one-loop level. We impose that the predicted values of the oblique parameters are in agreement with the fit result of Ref. [49] within 2σ confidence level.[1]

Regarding the description of the excesses at about 95 GeV, 2HDM + singlet models like the S2HDM provide a rather generic framework representative of a wide class of models with extended scalar sectors. In our numerical analysis, we applied the Planck measurement of today's relic abundance of $h^2\Omega = 0.119$ [52] as an upper limit, hence preventing an overclosure of the Universe but allowing for an under-abundance of the predicted DM. We used micrOMEGAs [53] for the calculation of the predicted relic abundance, assuming a standard cosmological history. We additionally applied the most stringent DM direct-detection limits from the LUX-ZEPLIN experiment [54] using the predictions for the DM-nucleon scattering cross sections at one-loop level computed in Ref. [55]. We note that fulfilling the condition of being in agreement with the applied DM constraints and the condition of describing the diphoton excess at 95 GeV can be satisfied simultaneously since the constraints mainly affect different sectors of the model. The only exception is that the combined effect of the constraint from the DM relic abundance, the signal-rate measurements of the detected Higgs boson at 125 GeV, and demanding compatibility with the 95 GeV excesses excludes parameter points for which the decay $h_{125} \to \chi\chi$ is kinematically open.

[1]We do not consider the recent CDF measurement of M_W [51] here; see the discussion in Ref. [36].

III. NUMERICAL ANALYSIS

In order to investigate the impact of the increased sensitivity in the diphoton channel due to the combination of ATLAS and CMS data in the S2HDM interpretation, we performed a parameter scan in the Yukawa types II and IV of the S2HDM. We analyzed the theoretical predictions in comparison to the experimental results for the observed excesses near 95 GeV, ensuring at the same time that the properties of h_{125} are in good agreement with the most up-to-date LHC signal rate measurements. We quantify the compatibility with the excesses at 95.4 GeV using the contributions $\chi^2_{\gamma\gamma}$, χ^2_{bb}, and $\chi^2_{\tau\tau}$, which are defined as

$$\chi^2_{\gamma\gamma,\tau\tau,bb} = \frac{\left(\mu_{\gamma\gamma,\tau\tau,bb} - \mu^{\mathrm{exp}}_{\gamma\gamma,\tau\tau,bb}\right)^2}{\left(\Delta\mu^{\mathrm{exp}}_{\gamma\gamma,\tau\tau,bb}\right)^2}. \tag{5}$$

For the experimental central values and the uncertainties, we use the values stated in Sec. I, and $\mu_{\gamma\gamma,\tau\tau,bb}$ are the theoretically predicted values. Since $\mu^{\mathrm{exp}}_{\gamma\gamma}$ has asymmetric uncertainties, we define $\chi^2_{\gamma\gamma}$ in such a way that the lower uncertainty is used if $\mu_{\gamma\gamma} < \mu^{\mathrm{exp}}_{\gamma\gamma}$, and the upper uncertainty is used if $\mu_{\gamma\gamma} > \mu^{\mathrm{exp}}_{\gamma\gamma}$. To obtain the predictions for $\mu_{\gamma\gamma}$ and $\mu_{\tau\tau}$, we used HiggsTools to derive the gluon-fusion cross section of the state at 95 GeV via a rescaling of the SM predictions as a function of $c_{h_{95}t\bar{t}}$ and $c_{h_{95}b\bar{b}}$. To compute μ_{bb}, we approximated the cross section ratio as $\sigma/\sigma_{\mathrm{SM}} = c^2_{h_{95}VV}$. The branching ratios of h_{95} were obtained with the help of N2HDECAY [56,57]. For the generation of the S2HDM parameter points and the application of the constraints, we used the program s2hdmTools [32,55], which features interfaces to HiggsTools, micrOMEGAs, and N2HDECAY.

A. Genetic algorithm

We scanned the S2HDM parameter space using a genetic algorithm in order to determine the parameter regions that are suitable for the description of the diphoton excess while being in agreement with the various theoretical and experimental constraints discussed above. Genetic algorithms mimic the process of natural selection to find solutions for problems whose solution space can be quantified in terms of a fitness function that needs to be maximized. The application of the genetic algorithm significantly improved the running time required to find

a valid parameter point compared to a random sampling of the model parameters. Compared to other optimization techniques, e.g., Markov Chain Monte Carlo algorithms or multimodal nested sampling algorithms, genetic algorithms are particularly well suited for the task at hand. This is due to the fact that they are derivative free and can be applied to nondifferentiable optimization problems as present here due to discrete constraints, such as the boundedness-from-below conditions or the 95% confidence-level cross section limits from BSM scalar searches. In addition, genetic algorithms are easily parallelizable, and they are particularly well suited to uncover novel and unconventional solutions to a problem as a result of the mating and mutation steps, as detailed below. Before discussing the specifics of the algorithm used in our analysis, we state the scan ranges of the free parameters.

The mass of h_{95} has been varied in the region in which the diphoton excess is most pronounced, i.e., 94 GeV $\leq m_{h_{95}} \leq 97$ GeV. The mass of the second-lightest Higgs boson has been set to $m_{h_{125}} = 125.09$ GeV. The masses of the remaining neutral and charged Higgs bosons, denoted as H, A, and $H^{\pm}$ in the following, as well as the mass of the DM state, have been scanned up to an upper limit of 1 TeV. For the mass of $H^{\pm}$, additionally the lower limit $m_{H^{\pm}} > 600$ GeV has been applied due to flavor-physics constraints, see above. Moreover, we have varied $\tan\beta$ in the range $1.5 \leq \tan\beta \leq 10$, and for the singlet vev, we have chosen 40 GeV $\leq v_S \leq 2$ TeV. Finally, the scan range of the parameter m_{12}^2 has been determined by the condition 400 GeV $\leq M \leq 1$ TeV, where $M^2 = m_{12}^2/(\sin\beta\cos\beta)$.

For the implementation of the genetic algorithm, we used the software package DEAP [58]. As a starting point for obtaining parameter points that describe the observed excesses and that are in agreement with the constraints, we created a so-called population of 500,000 parameter points, called individuals, where each individual is defined by a list of floating point numbers corresponding to the values of the free parameters. This list can be thought of as the chromosome of an individual. The chromosomes of the individuals of the initial population were generated by randomly assigning the values of the free parameters within the scan ranges given above.

The goodness of fit of each parameter point is quantified in terms of a so-called fitness function whose value becomes larger with increasing quality of the fit. We defined a fitness function depending on the compatibility with the observed excesses in terms of $\chi^2_{\gamma\gamma}$, $\chi^2_{\tau\tau}$, and χ^2_{bb}, on the compatibility with the signal-rate measurements of the Higgs boson at 125 GeV in terms of χ^2_{125}, and by piecewise assigning large penalties to the fitness if any of the theoretical or other experimental constraints were violated. The genetic algorithm operates by progressively generating new generations of individuals through combining the traits of individuals from the previous generation. This *crossover* procedure is defined in such a way that the fitness of the individuals from one generation to the other is improved, and it works in three steps:

The first step is called selection, where based on the fitness of the individuals, a subset of the population is selected that is allowed to participate in the production of new individuals, called offsprings. In our parameter scan, we used tournament selection with size $k = 3$; i.e., from the existing population, three individuals are randomly drawn, and only the individual with the best fitness is selected to be able to participate in the subsequent step. This is done until a selected population of 500,000 is achieved. Since the same individual can be selected more than once, the number of selected individuals is in general smaller than the total number of individuals in the original population.

The second step of the crossover procedure is the mating stage. The mating stage creates new individuals whose chromosomes are inherited from the subset of the previously selected individuals. We used uniform crossover with two parent individuals, where each element of the chromosome of the offspring is taken over randomly from one of the two parent individuals. By empirically studying the rate of increase of the fitness values, we found that the performance of the algorithm is improved if a dominant part of the parameter values is taken over from one of the parents. Conversely, mixing the parameter values from both parents in equal amounts often results in offsprings with poor fitness, where the corresponding parameter point violates at least one of the theoretical or experimental constraints due to significant changes in too many parameters. We therefore set a probability of 80% for each element of the chromosome of the offspring to come from one of the parents and 20% from the other parent. With the mating procedure, we produced a total number of 500,000 offsprings.

The third and final step of the crossover procedure is the mutation stage. At this state, a randomly chosen subset of the new population is exposed to a modification of their chromosomes. The mutation stage is especially important to maintain diversity in the population and thus for the coverage of a large region of the solution space by preventing that the algorithm becomes trapped in local maxima of the fitness function. In our scan, 10% of the population was chosen to be exposed to mutation. The chromosome of an individual was mutated by replacing each element with a probability of 10% with a float number that was randomly chosen within an interval between 0.8 and 1.2 times the original value. After the mutation stage, the production of the new generation of the population is complete.

We let the algorithm evolve for a total number of 40 generations. In order not to lose the individual with the best fitness at intermediate stages due to the mating or mutation steps, the best-fit individual was always appended separately to the new generation of individuals without any

modification to its chromosome. At the end of the evolution, the individual with the best fitness was saved; i.e., we ran the genetic algorithm once for each parameter point contained in our final sample displayed in the plots. Each run of the genetic algorithm took about one hour on a typical CPU. Running the algorithm in parallel on a 48-CPU cluster enabled us to efficiently obtain the final sample of parameter points discussed in our analysis within a few days. These points adhere to all applied constraints and have been selected based on their compatibility with the observed excesses at 95 GeV.

B. Analysis of the diphoton excess

In Fig. 1, we show the predictions for $\mu_{\gamma\gamma}$ for the S2HDM parameter points that are in agreement with the applied constraints. The type II parameter points are shown in blue, and the parameter points of type IV are shown in orange. It should be noted that the orange points are plotted above the blue ones; i.e., the whole range displayed for the orange points is also covered by the blue points. The expected and observed cross section limits obtained by CMS are indicated by the black dashed and solid lines, respectively. The 1σ and 2σ uncertainty bands are indicated by the green and yellow bands, respectively [13]. Overlaid are the expected and observed 95% confidence-level limits on the signal strengths observed by ATLAS [14] as dashed and solid red lines, respectively. We obtained these limits by normalizing the expected and observed cross-section limits reported by ATLAS with the cross sections predicted for a SM Higgs boson at the same mass [30] using HiggsTools [45]. The values of $\mu_{\gamma\gamma}^{\text{ATLAS}}$, $\mu_{\gamma\gamma}^{\text{CMS}}$, and $\mu_{\gamma\gamma}^{\text{ATLAS+CMS}}$ and their respective uncertainties are indicated by the red, black (left plot), and cyan (right plot) error bars at 95.4 GeV. One can see that both types of the S2HDM considered here can accommodate the combined observed excess. Type II can give rise to larger predicted values of $\mu_{\gamma\gamma}$ due to a suppression of the $h_{95} \to \tau^+\tau^-$ decay mode; see the discussion in Ref. [26].

C. Diphoton vs $b\bar{b}$ vs $\tau^+\tau^-$ excesses

In the previous subsection, we demonstrated that both the Yukawa types II and IV can describe the excess in the diphoton channel observed by ATLAS and CMS. Now we turn to the question of whether additionally the $b\bar{b}$ excess observed at LEP and/or the $\tau^+\tau^-$ excess at CMS can be accommodated.

Starting with the $b\bar{b}$ excess, we show in the top row of Fig. 2 the parameter points passing the applied constraints in the $(\mu_{\gamma\gamma}, \mu_{bb})$ plane. The parameter points of type II and type IV are shown in the left and the right plot, respectively. The colors of the points indicate the value of $\Delta\chi^2_{125}$, quantifying the degree of compatibility with the LHC rate measurements of h_{125}. The black dashed lines indicate the region in which the excesses are described at a level of 1σ or better; i.e., $\chi^2_{\gamma\gamma} + \chi^2_{bb} \leq 2.3$ [see Eq. (5)]. The corresponding gray dot-dashed lines indicate the previous result based solely on the CMS Run 2 data regarding the diphoton excess.

One can observe that there are points inside the 1σ preferred region in the upper left and right plots. Thus, both type II and type IV are able to describe the increased sensitivity in the diphoton channel, now reaching 3.1σ and the $b\bar{b}$ excess simultaneously. At the same time, the properties of the second-lightest scalar h_{125} are such that the LHC rate measurements can be accommodated at the same χ^2 level as in the SM, i.e., $\Delta\chi^2_{125} \approx 0$, or better. Such points are found inside the 1σ preferred region for μ_{bb} values below the central value. At the current level of experimental precision, the description of both excesses is therefore possible in combination with the presence of a Higgs boson at 125 GeV that would so far be indistinguishable from a SM Higgs boson.

Turning to the di-tau excess, we show in the bottom row of Fig. 2 the parameter points passing the applied constraints in the $(\mu_{\gamma\gamma}, \mu_{\tau\tau})$ plane. As before, the colors of the points indicate the values of $\Delta\chi^2_{125}$. The black dashed lines indicate the region in which the diphoton excess and the di-tau excess are described at a level of 1σ or better, i.e., $\chi^2_{\gamma\gamma} + \chi^2_{\tau\tau} \leq 2.3$, whereas the gray dot-dashed line corresponds to the preferred 1σ region based solely on the CMS result regarding the diphoton excess.

In the lower left plot, showing the parameter points of the scan in type II, one can see that there are no points within or close to the 1σ region. This finding can be understood from the discussion in Sec. II B. The conclusion that the two excesses cannot be simultaneously described in this case is qualitatively unchanged as compared to the results of Refs. [26,35], where $\mu_{\gamma\gamma}^{\text{exp}} = 0.6 \pm 0.2$ and $0.33^{+0.19}_{-0.12}$ were used, respectively.

The lower right plot shows the parameter points passing the applied constraints from the scan in type IV. One can observe that the values of $\mu_{\tau\tau}$ overall increase with increasing values of $\mu_{\gamma\gamma}$. While some parameter points reach the lower edge of the black 1σ line, the new result for $\mu_{\gamma\gamma}$ worsens the simultaneous compatibility with the diphoton and the di-tau excess for the type IV case as compared to the previous result for the diphoton excess that was based solely on the CMS result. Regarding the di-tau excess, all points lie substantially below the central value of $\mu_{\tau\tau}^{\text{exp}}$. Although larger values of $\mu_{\tau\tau}$ can theoretically be achieved in type IV [35], such parameter points are excluded by experimental bounds from recent searches performed by CMS for the production of a Higgs boson in association with a top-quark pair or in association with a Z boson, with subsequent decay into tau pairs [59]. In addition, in the S2HDM, values of $\mu_{\tau\tau} \gtrsim 0.7$ are in tension with cross section limits from Higgs-boson searches at LEP for the decay of the Higgs boson into a pair of

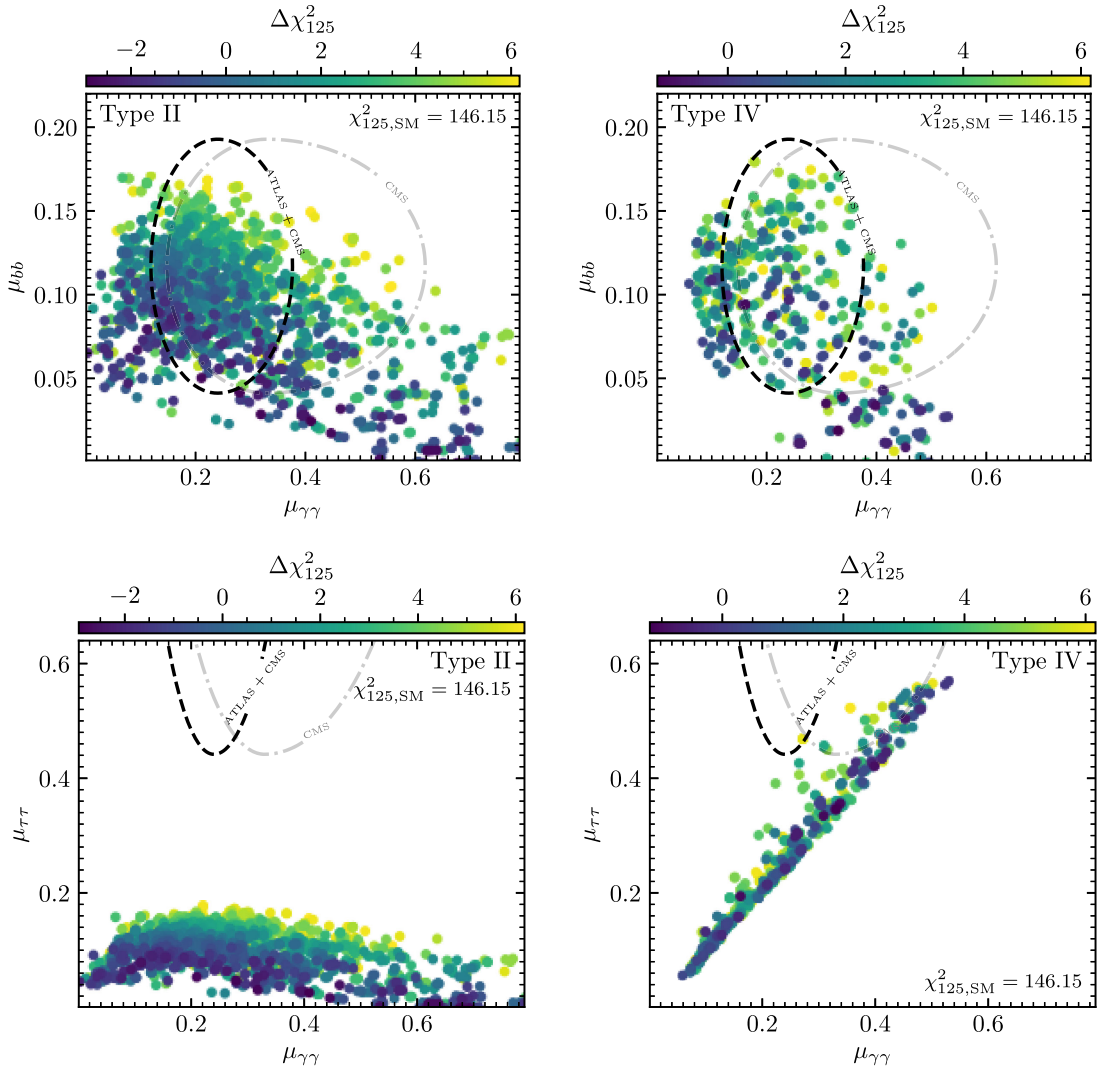

FIG. 2. S2HDM parameter points passing the applied constraints in the $(\mu_{\gamma\gamma}, \mu_{bb})$ plane (top row) and the $(\mu_{\gamma\gamma}, \mu_{\tau\tau})$ plane (bottom row) for type II (left) and type IV (right). The colors of the points indicate the value of $\Delta\chi^2_{125}$. The black dashed lines indicate the regions in which the two excesses considered in each plot are accommodated at a level of 1σ or better; i.e., $\chi^2_{\gamma\gamma} + \chi^2_{bb} \leq 2.3$ (top row) and $\chi^2_{\gamma\gamma} + \chi^2_{\tau\tau} \leq 2.3$ (bottom row). The corresponding gray dot-dashed lines indicate the previous result based solely on the CMS Run 2 data.

τ leptons [4,35]. Consequently, a simultaneous description of the $\gamma\gamma$ and the $\tau\tau$ excesses is possible at best at the level of 1σ. We note here that a better description of both the diphoton and the di-tau excess can be achieved if h_{95} is identified with a CP-odd state [27] because such a scenario is less constrained by the limits arising from top-quark associated production (see also Ref. [37]).

In Table I, we provide details of a selection of three benchmark points that we obtained in our parameter scan in the type II S2HDM. These benchmark points feature a very good description of the diphoton excess observed at the LHC in combination with the $b\bar{b}$ excess observed at LEP, while the excess of di-tau events observed by CMS cannot be described in type II as discussed above. Moreover, the benchmark points BP1 and BP3 saturate the measured DM relic abundance, while the DM density predicted for BP2 is underabundant, leaving room for additional components contributing to the observed DM relic abundance. For BP1, the DM state χ has a mass of $m_\chi = 63.3$ GeV, thus annihilating efficiently via s channel exchange of h_{125}, while the invisible decay $h_{125} \to \chi\chi$ is still kinematically closed for the on-shell case.[2] For BP3, χ is substantially heavier, $m_\chi = 964$ GeV, and annihilates mainly via processes involving the heavy BSM states h_3 and A.

[2]Such a scenario is especially compelling in view of the excess of gamma rays from the galactic center observed by the Fermi Large Area Telescope [60–62]. A possible origin of this long-standing excess could be the annihilation of a WIMP DM candidate in this mass window [63,64], potentially in agreement with the properties of the DM state χ for BP1 (see Ref. [32] for a detailed discussion).

TABLE I. Selection of benchmark points from the scan in type II that describe the diphoton excess observed at the LHC and the $b\bar{b}$ excess observed at LEP, while being in agreement with all other experimental and theoretical constraints. BP1 and BP3 additionally saturate the measured relic abundance of DM, whereas for BP2, the predicted DM density is underabundant.

Benchmark points: Type II

Parameters	$\tan\beta$	α_1	α_2	α_4	m_{h_1}	m_{h_2}	m_{h_3}	m_A	$m_{H^\pm}$	m_χ	v_s	M
BP1	2.79	1.35	1.22	1.49	95.7	125	687	812	658	63.3	1674	664
BP2	3.65	1.39	1.20	1.52	95.1	125	556	681	669	276	843	548
BP3	3.30	1.41	1.25	1.46	95.9	125	785	848	849	964	600	770

Phenomenology	$\mu_{\gamma\gamma}$	μ_{bb}	$\mu_{\tau\tau}$	$\Delta\chi^2_{125}$	$h^2\Omega$
BP1	0.247	9.94×10^{-2}	9.62×10^{-2}	−0.467	0.114
BP2	0.245	0.118	0.109	2.10	4.67×10^{-3}
BP3	0.243	7.73×10^{-2}	7.43×10^{-2}	1.74	0.104

Branching ratios

h_1	$b\bar{b}$	$\tau^+\tau^-$	WW	ZZ	$\gamma\gamma$
BP1	0.690	6.99×10^{-2}	1.01×10^{-2}	1.38×10^{-3}	2.74×10^{-3}
BP2	0.717	7.27×10^{-2}	8.39×10^{-3}	1.20×10^{-3}	2.44×10^{-3}
BP3	0.644	6.52×10^{-2}	1.26×10^{-2}	1.70×10^{-3}	3.26×10^{-3}

h_2	$b\bar{b}$	$\tau^+\tau^-$	WW	ZZ	$\gamma\gamma$
BP1	0.543	5.83×10^{-2}	0.238	2.98×10^{-2}	2.61×10^{-3}
BP2	0.532	5.71×10^{-2}	0.246	3.08×10^{-2}	2.61×10^{-3}
BP3	0.570	6.52×10^{-2}	0.222	2.78×10^{-2}	2.41×10^{-3}

h_3	$t\bar{t}$	h_2h_2	h_1h_2	WW	ZZ	h_1h_1
BP1	0.688	0.117	7.09×10^{-2}	5.93×10^{-2}	2.89×10^{-2}	9.32×10^{-3}
BP2	0.631	0.123	6.24×10^{-2}	5.71×10^{-2}	2.73×10^{-2}	1.06×10^{-2}
BP3	0.766	5.27×10^{-2}	7.06×10^{-2}	2.99×10^{-2}	1.47×10^{-2}	2.05×10^{-2}

A	$W^\pm H^\mp$	$t\bar{t}$	Zh_3	Zh_1	Zh_2
BP1	0.566	0.313	8.25×10^{-2}	1.88×10^{-2}	1.21×10^{-2}
BP2		0.604	0.312	2.21×10^{-2}	2.33×10^{-2}
BP3		0.881	7.43×10^{-2}	7.92×10^{-3}	3.33×10^{-3}

$H^\pm$	tb	Wh_1	Wh_2	Wh_3
BP1	0.936	3.68×10^{-2}	2.32×10^{-2}	
BP2	0.657	2.33×10^{-2}	2.45×10^{-2}	0.289
BP3	0.908	7.68×10^{-2}	8.28×10^{-3}	

Effective couplings	c_{h_1VV}	$c_{h_1t\bar{t}}$	$c_{h_1b\bar{b}}$	c_{h_2VV}	$c_{h_2t\bar{t}}$	$c_{h_2b\bar{b}}$	c_{h_3VV}	$c_{h_3t\bar{t}}$	$c_{h_3b\bar{b}}$
BP1	0.340	0.355	0.221	−0.939	−0.952	−0.843	4.69×10^{-2}	−0.311	2.83
BP2	0.363	0.371	0.251	−0.931	−0.940	−0.813	4.12×10^{-2}	−0.232	3.689
BP3	0.310	0.322	0.177	−0.950	−0.955	−0.906	2.52×10^{-2}	−0.277	3.324

A typical feature of the parameter points describing the diphoton excess is the suppression of the couplings of h_{95} and h_{125} to down-type quarks compared to the couplings to up-type quarks. Regarding the phenomenology of the heavier scalars, typically the third CP-even scalar h_3 is lighter than the CP-odd state A and the charged scalars $H^\pm$. If the mass splitting is sufficiently large, e.g., for BP2, searches for signals like $A \to Zh_3$ and $H^\pm \to W^\pm h_3$ can be

TABLE II. Selection of benchmark points from the scan in type IV that describe the diphoton excess observed at the LHC and the $b\bar{b}$ excess observed at LEP, while being in agreement with all other experimental and theoretical constraints. BP1 and BP3 additionally predict a relic abundance of DM that is close to the measured value, whereas for BP2, the predicted DM density is underabundant.

Benchmark point: Type IV

Parameters	$\tan\beta$	α_1	α_2	α_4	m_{h_1}	m_{h_2}	m_{h_3}	m_A	$m_{H^\pm}$	m_χ	v_s	M
BP1	7.38	−1.50	−1.18	−1.39	95.2	125	918	903	834	517	674	918
BP2	4.19	1.44	1.15	1.51	95.9	125	742	785	778	314	132	739
BP3	3.14	1.43	1.19	1.44	95.2	125	578	838	842	312	488	580

Phenomenology	$\mu_{\gamma\gamma}$	μ_{bb}	$\mu_{\tau\tau}$	$\Delta\chi^2_{125}$	$h^2\Omega$
BP1	0.304	9.34×10^{-2}	0.353	0.227	0.0777
BP2	0.382	0.117	0.412	3.03	1.22×10^{-2}
BP3	0.343	7.50×10^{-2}	0.414	5.55	0.107

Branching ratios

h_1	$b\bar{b}$	$\tau^+\tau^-$	WW	ZZ	$\gamma\gamma$
BP1	0.544	0.183	9.75×10^{-3}	1.38×10^{-3}	2.66×10^{-3}
BP2	0.554	0.189	1.15×10^{-2}	1.54×10^{-2}	3.01×10^{-3}
BP3	0.458	0.231	1.18×10^{-2}	1.66×10^{-3}	3.21×10^{-3}

h_2	$b\bar{b}$	$\tau^+\tau^-$	WW	ZZ	$\gamma\gamma$
BP1	0.514	7.54×10^{-2}	0.247	3.09×10^{-2}	2.76×10^{-3}
BP2	0.511	7.64×10^{-2}	0.247	3.09×10^{-2}	2.68×10^{-2}
BP3	0.544	7.14×10^{-2}	0.231	2.89×10^{-2}	2.41×10^{-2}

h_3	$t\bar{t}$	h_2h_2	h_1h_2	WW	h_1h_1	$W^\pm H^\mp$	$\chi\chi$
BP1	8.64×10^{-2}	0.181	0.299	0.145	7.38×10^{-4}	2.24×10^{-2}	
BP2	0.376	0.206	6.43×10^{-2}	9.56×10^{-2}	0.113		3.12×10^{-2}
BP3	0.637	0.103	0.103	5.52×10^{-2}	3.45×10^{-2}		

A	$b\bar{b}$	$t\bar{t}$	Zh_1	Zh_2	Zh_3
BP1	0.226	0.262	0.383	2.39×10^{-2}	
BP2	7.03×10^{-2}	0.773	0.102	5.24×10^{-2}	
BP3	4.08×10^{-3}	0.143	2.42×10^{-2}	4.23×10^{-2}	0.824

$H^\pm$	tb	Wh_1	Wh_2	Wh_3
BP1	0.518	0.459	2.26×10^{-2}	
BP2	0.840	0.105	5.38×10^{-2}	
BP3	0.133	2.31×10^{-2}	4.04×10^{-3}	0.839

Effective couplings	c_{h_1VV}	$c_{h_1t\bar{t}}$	$c_{h_1b\bar{b}}$	c_{h_2VV}	$c_{h_2t\bar{t}}$	$c_{h_2b\bar{b}}$	c_{h_3VV}	$c_{h_3t\bar{t}}$	$c_{h_3b\bar{b}}$
BP1	−0.371	−0.381	0.212	0.928	0.930	0.796	4.59×10^{-2}	-8.91×10^{-2}	7.40
BP2	0.410	0.421	0.229	−0.911	−0.918	−0.778	4.66×10^{-2}	−0.192	4.23
BP3	0.362	0.381	0.171	−0.931	−0.939	−0.850	4.62×10^{-2}	−0.272	3.18

utilized to probe the preferred parameter space regions. This is of particular interest since the parameter space regions where these channels are kinematically open are also favored by the presence of a first-order EW phase transition in SM extensions containing a second Higgs doublet [65]. Due to the required departures from the alignment limit in order to produce sizable signal rates for the state h_{95}, the parameter space relevant for a description

of the diphoton excess may also be probed via searches for otherwise strongly suppressed decays of $A \to Zh_{125}$ or searches for the decay $H \to h_{125}h_{125}$. For the latter, we find branching ratios at the level of 10%, see BP1 and BP2 in Table I.

In Table II, we provide a similar selection of benchmark points from the scan in the S2HDM of type IV. Compared to the type II parameter points, these parameter points feature also sizable signal rates of h_{95} in the di-tau decay mode. However, as discussed above, the predicted signal rates of $\mu_{\tau\tau} \approx 0.4$ are still substantially below the experimentally observed value of $\mu_{\tau\tau}^{\text{exp}} = 1.2 \pm 0.5$, while at the same time, the signal rates for the diphoton excess $\mu_{\gamma\gamma}$ are predicted to be slightly larger than the best-fit values in this parameter region (as is also visible in the lower right plot of Fig. 2). The parameter space regions preferred for a description of the diphoton excess are overall similar to the ones found for type II, with the exception that in type IV, it is possible to reach larger values of $\tan\beta$. This is a consequence of the fact that in type IV, the bounds from LHC searches for heavy Higgs bosons decaying into τ-lepton pairs are weaker [11,66] because the couplings of A and of H to charged leptons are suppressed by factors of $1/\tan\beta$, whereas these couplings are enhanced in type II by factors of $\tan\beta$. No relevant distinction occurs between the two types concerning the DM phenomenology. As in type II, the predicted DM relic density can account for the observed DM abundance (or of a large part of it), e.g., for BP1 and BP3 shown in Table II, while at the same time, the diphoton excess and the $b\bar{b}$ excess observed at LEP can be described in good agreement with the observed signal rates. Still, it is also possible that the predicted DM abundance is orders of magnitude below the observed one, for instance, for BP2, where the DM mass $m_\chi = 276$ GeV is very close to half the mass of the heavy CP-even scalar, $m_{h_3} = 556$ GeV, such that the annihilation of χ in the early Universe is resonantly enhanced (the branching ratio for the decay $h_3 \to \chi\chi$ is also given in Table II).

IV. CONCLUSIONS AND OUTLOOK

Recently, upon the inclusion of the full Run 2 dataset and improved analysis techniques, resulting in a substantially improved sensitivity compared to the previous analysis, the ATLAS collaboration has reported an excess of 1.7σ local significance at about 95.4 GeV in the low-mass Higgs boson searches in the diphoton final state. An excess in the same channel at the same mass value and with higher local significance of 2.9σ had previously been found by CMS based on the Run 2 dataset, and an excess with similar significance had also been observed already in the CMS diphoton searches at 8 TeV. Neglecting possible correlations, we obtain a combined signal strength of $\mu_{\gamma\gamma}^{\text{ATLAS+CMS}} = 0.24^{+0.09}_{-0.08}$, corresponding to an excess of 3.1σ for the mass value of $m_\phi \equiv m_\phi^{\text{ATLAS+CMS}} = 95.4$ GeV.

We have investigated the interpretation of the combined result from ATLAS and CMS as a diphoton resonance arising from the production of a Higgs boson in the Two-Higgs doublet model that is extended by a complex singlet (S2HDM). Using a genetic algorithm, we scanned the parameter space of the model in order to determine parameter regions that feature a scalar state at 95 GeV with sizable signal rates in the processes in which the excesses have appeared. We have shown that a good description of the excess that is in line with the slightly increased significance of the combination in comparison to the previous result from CMS is possible in the Yukawa types II and IV, while being in agreement with all other collider searches for additional Higgs bosons, the measurements of the properties of the SM-like Higgs boson at 125 GeV, and further experimental and theoretical constraints. At the same time, the model can account for the observed DM relic abundance in agreement with the measurements of the Planck satellite.

The diphoton excess observed at ATLAS and CMS is especially intriguing in view of additional excesses that appeared at approximately the same mass. Investigating this possibility, we have demonstrated that the S2HDM of type II can simultaneously describe the ATLAS/CMS diphoton excess and the $b\bar{b}$ excess observed at LEP, whereas no significant signal for the CMS di-tau excess is possible in this model. In the S2HDM of type IV, on the other hand, in addition, also a sizable signal strength in the di-tau channel can occur, but with maximally reachable signal rates somewhat below the signal strengths that would be required to describe the di-tau excess at the level of 1σ.

It should be noted in this context that our results in the S2HDM can be generalized to other extended Higgs sectors containing a SM-like Higgs boson and at least a second Higgs doublet as well as at least one singlet with a Higgs boson at about 95.4 GeV.

In the near future, the possible presence of a Higgs boson at about 95.4 GeV can be probed by the eagerly awaited update of the ATLAS searches in the di-tau final states covering the mass region below 125 GeV. Furthermore, the Run 3 results from ATLAS and CMS in the diphoton channel near 95 GeV will shed light on the question of whether the excesses that have been observed by ATLAS and CMS in the diphoton channel have been a first sign of a new particle. Further into the future, the existence of a possible state h_{95} will be tested in a twofold way at future runs of the (HL)-LHC, where the direct searches for h_{95} in different channels and the coupling measurements of h_{125} will benefit in particular from a significant increase of statistics. However, it was demonstrated in Ref. [26] that the experimental precision of the coupling measurements of the Higgs boson at 125 GeV might not be sufficient to exclude the S2HDM interpretation of the excesses at 95.4 GeV or conversely confirm a deviation from the SM

predictions. On the other hand, a future e^+e^- collider could determine the couplings of h_{125} to a sufficiently high precision [26]. Despite the suppressed couplings of the possible state at 95.4 GeV compared to h_{125}, a future e^+e^- Higgs factory could produce h_{95} in large numbers if it has a sufficiently large coupling to Z bosons, see, e.g., Ref. [67], and determine its properties with high precision.

In summary, the simultaneous observation of excesses in the $\gamma\gamma$ channel at the same mass value of 95.4 GeV at both ATLAS and CMS (together with the other observed excesses that are compatible with this mass value) gives rise to the intriguing possibility that a particle that cannot be accommodated by the SM of particle physics could be discovered in the near future.

ACKNOWLEDGMENTS

We thank M. Martínez for helpful discussion on the combination of the data. S. H. thanks the CTPU (Particle Theory and Cosmology Group) at the IBS (Daejeon, South Corea) for hospitality during the final stages of this work. G. W. acknowledges support by the Deutsche Forschungsgemeinschaft (DFG, German Research Foundation) under Germany's Excellence Strategy—EXC 2121 "Quantum Universe"—390833306. The work of G. W. has been partially funded by the Deutsche Forschungsgemeinschaft (DFG, German Research Foundation)—491245950. S. H acknowledges support from the grant IFT Centro de Excelencia Severo Ochoa CEX2020-001007-S funded by MCIN/AEI/10.13039/501100011033. The work of S. H. was supported in part by the grant PID2019–110058 GB-C21 funded by MCIN/AEI/10.13039/501100011033 and by "ERDF A way of making Europe." The work of T. B. is supported by the German Bundesministerium für Bildung und Forschung (BMBF, Federal Ministry of Education and Research)—Project No. 05H21VKCCA.

[1] ATLAS Collaboration, Observation of a new particle in the search for the Standard Model Higgs boson with the ATLAS detector at the LHC, Phys. Lett. B **716**, 1 (2012).
[2] CMS Collaboration, Observation of a new boson at a mass of 125 GeV with the CMS experiment at the LHC, Phys. Lett. B **716**, 30 (2012).
[3] OPAL Collaboration, Decay mode independent searches for new scalar bosons with the OPAL detector at LEP, Eur. Phys. J. C **27**, 311 (2003).
[4] LEP Working Group for Higgs Boson Searches, ALEPH, DELPHI, L3, and OPAL Collaborations, Search for the standard model Higgs boson at LEP, Phys. Lett. B **565**, 61 (2003).
[5] ALEPH, DELPHI, L3, OPAL, and LEP Working Group for Higgs Boson Searches Collaborations, Search for neutral MSSM Higgs bosons at LEP, Eur. Phys. J. C **47**, 547 (2006).
[6] CDF and D0 Collaborations, Updated combination of CDF and D0 searches for standard model Higgs boson production with up to 10.0 fb^{-1} of data, arXiv:1207.0449.
[7] CMS Collaboration, Search for new resonances in the diphoton final state in the mass range between 80 and 110 GeV in pp collisions at $\sqrt{s} = 8$ TeV, Technical Report No. CMS-PAS-HIG-14-037, 2015, https://cds.cern.ch/record/2063739.
[8] CMS Collaboration, Search for a standard model-like Higgs boson in the mass range between 70 and 110 GeV in the diphoton final state in proton-proton collisions at $\sqrt{s} = 8$ and 13 TeV, Phys. Lett. B **793**, 320 (2019).
[9] CMS Collaboration, Search for additional neutral MSSM Higgs bosons in the $\tau\tau$ final state in proton-proton collisions at $\sqrt{s} = 13$ TeV, J. High Energy Phys. 09 (2018) 007.
[10] ATLAS Collaboration, Search for resonances in the 65 to 110 GeV diphoton invariant mass range using 80 fb^{-1} of pp collisions collected at $\sqrt{s} = 13$ TeV with the ATLAS detector, Technical Report No. ATLAS-CONF-2018-025, 2018, https://cds.cern.ch/record/2628760.
[11] CMS Collaboration, Searches for additional Higgs bosons and for vector leptoquarks in $\tau\tau$ final states in proton-proton collisions at $\sqrt{s} = 13$ TeV, J. High Energy Phys. 07 (2023) 073.
[12] ATLAS Collaboration, Search for boosted diphoton resonances in the 10 to 70 GeV mass range using 138 fb^{-1} of 13 TeV pp collisions with the ATLAS detector, J. High Energy Phys. 07 (2023) 155.
[13] CMS Collaboration, Search for low mass resonances in the diphoton final state in proton-proton collisions at $\sqrt{s} =$ 13 TeV with the full Run 2 dataset, Technical Report No. CMS-HIG-20-002, 2023, https://cds.cern.ch/record/2852907.
[14] ATLAS Collaboration, Search for diphoton resonances in the 66 to 110 GeV mass range using 140 fb^{-1} of 13 TeV pp collisions collected with the ATLAS detector, Technical Report No. ATLAS-CONF-2023-035, CERN, Geneva, 2023, https://cds.cern.ch/record/2862024.
[15] J. Cao, X. Guo, Y. He, P. Wu, and Y. Zhang, Diphoton signal of the light Higgs boson in natural NMSSM, Phys. Rev. D **95**, 116001 (2017).
[16] P. J. Fox and N. Weiner, Light signals from a lighter Higgs, J. High Energy Phys. 08 (2018) 025.
[17] F. Richard, Search for a light radion at HL-LHC and ILC250, arXiv:1712.06410.
[18] U. Haisch and A. Malinauskas, Let there be light from a second light Higgs doublet, J. High Energy Phys. 03 (2018) 135.
[19] T. Biekötter, S. Heinemeyer, and C. Muñoz, Precise prediction for the Higgs-boson masses in the $\mu\nu$ SSM, Eur. Phys. J. C **78**, 504 (2018).

[20] D. Liu, J. Liu, C. E. M. Wagner, and X.-P. Wang, A light Higgs at the LHC and the B-anomalies, J. High Energy Phys. 06 (2018) 150.
[21] F. Domingo, S. Heinemeyer, S. Paßehr, and G. Weiglein, Decays of the neutral Higgs bosons into SM fermions and gauge bosons in the $\mathcal{CP}$-violating NMSSM, Eur. Phys. J. C **78**, 942 (2018).
[22] T. Biekötter, M. Chakraborti, and S. Heinemeyer, A 96 GeV Higgs boson in the N2HDM, Eur. Phys. J. C **80**, 2 (2020).
[23] J. M. Cline and T. Toma, Pseudo-Goldstone dark matter confronts cosmic ray and collider anomalies, Phys. Rev. D **100**, 035023 (2019).
[24] J. Cao, X. Jia, Y. Yue, H. Zhou, and P. Zhu, 96 GeV diphoton excess in seesaw extensions of the natural NMSSM, Phys. Rev. D **101**, 055008 (2020).
[25] J. A. Aguilar-Saavedra and F. R. Joaquim, Multiphoton signals of a (96 GeV?) stealth boson, Eur. Phys. J. C **80**, 403 (2020).
[26] T. Biekötter, S. Heinemeyer, and G. Weiglein, The CMS diphoton excess at 95 GeV in view of the LHC Run 2 results, Phys. Lett. B **846**, 138217 (2023).
[27] D. Azevedo, T. Biekötter, and P. M. Ferreira, 2HDM interpretations of the CMS diphoton excess at 95 GeV, J. High Energy Phys. 11 (2023) 017.
[28] T. Biekötter, Scalar extensions of the SM and recent experimental anomalies, in *Proceedings of the 57th Rencontres de Moriond on Electroweak Interactions and Unified Theories* (2023), 10.58027%2Fe6wg-ee33.
[29] C. Arcangeletti, ATLAS, LHC seminar, https://indico.cern.ch/event/1281604/ (2023).
[30] LHC Higgs Cross Section Working Group, Handbook of LHC Higgs cross sections: 4. Deciphering the nature of the Higgs sector, arXiv:1610.07922.
[31] A. Azatov, R. Contino, and J. Galloway, Model-independent bounds on a light Higgs, J. High Energy Phys. 04 (2012) 127.
[32] T. Biekötter and M. O. Olea-Romacho, Reconciling Higgs physics and pseudo-Nambu-Goldstone dark matter in the S2HDM using a genetic algorithm, J. High Energy Phys. 10 (2021) 215.
[33] T. Biekötter, A. Grohsjean, S. Heinemeyer, C. Schwanenberger, and G. Weiglein, Possible indications for new Higgs bosons in the reach of the LHC: N2HDM and NMSSM interpretations, Eur. Phys. J. C **82**, 178 (2022).
[34] S. Heinemeyer, C. Li, F. Lika, G. Moortgat-Pick, and S. Paasch, Phenomenology of a 96 GeV Higgs boson in the 2HDM with an additional singlet, Phys. Rev. D **106**, 075003 (2022).
[35] T. Biekötter, S. Heinemeyer, and G. Weiglein, Mounting evidence for a 95 GeV Higgs boson, J. High Energy Phys. 08 (2022) 201.
[36] T. Biekötter, S. Heinemeyer, and G. Weiglein, Excesses in the low-mass Higgs-boson search and the W-boson mass measurement, Eur. Phys. J. C **83**, 450 (2023).
[37] S. Iguro, T. Kitahara, and Y. Omura, Scrutinizing the 95–100 GeV di-tau excess in the top associated process, Eur. Phys. J. C **82**, 1053 (2022).
[38] X.-M. Jiang, C. Cai, Z.-H. Yu, Y.-P. Zeng, and H.-H. Zhang, Pseudo-Nambu-Goldstone dark matter and two-Higgs-doublet models, Phys. Rev. D **100**, 075011 (2019).
[39] G. C. Branco, P. M. Ferreira, L. Lavoura, M. N. Rebelo, M. Sher, and J. P. Silva, Theory and phenomenology of two-Higgs-doublet models, Phys. Rep. **516**, 1 (2012).
[40] R. Barbieri, D. Buttazzo, K. Kannike, F. Sala, and A. Tesi, One or more Higgs bosons?, Phys. Rev. D **88**, 055011 (2013).
[41] P. Bechtle, O. Brein, S. Heinemeyer, G. Weiglein, and K. E. Williams, HiggsBounds: Confronting arbitrary Higgs sectors with exclusion bounds from LEP and the Tevatron, Comput. Phys. Commun. **181**, 138 (2010).
[42] P. Bechtle, O. Brein, S. Heinemeyer, G. Weiglein, and K. E. Williams, HiggsBounds 2.0.0: Confronting neutral and charged Higgs sector predictions with exclusion bounds from LEP and the Tevatron, Comput. Phys. Commun. **182**, 2605 (2011).
[43] P. Bechtle, O. Brein, S. Heinemeyer, O. Stål, T. Stefaniak, G. Weiglein, and K. E. Williams, HiggsBounds-4: Improved tests of extended Higgs sectors against exclusion bounds from LEP, the Tevatron and the LHC, Eur. Phys. J. C **74**, 2693 (2014).
[44] P. Bechtle, D. Dercks, S. Heinemeyer, T. Klingl, T. Stefaniak, G. Weiglein, and Jonas Wittbrodt, HiggsBounds-5: Testing Higgs sectors in the LHC 13 TeV era, Eur. Phys. J. C **80**, 1211 (2020).
[45] H. Bahl, T. Biekötter, S. Heinemeyer, C. Li, S. Paasch, G. Weiglein, and J. Wittbrodt, HiggsTools: BSM scalar phenomenology with new versions of HiggsBounds and HiggsSignals, Comput. Phys. Commun. **291**, 108803 (2023).
[46] P. Bechtle, S. Heinemeyer, O. Stål, T. Stefaniak, and G. Weiglein, HiggsSignals: Confronting arbitrary Higgs sectors with measurements at the Tevatron and the LHC, Eur. Phys. J. C **74**, 2711 (2014).
[47] P. Bechtle, S. Heinemeyer, O. Stål, T. Stefaniak, and G. Weiglein, Probing the standard model with Higgs signal rates from the Tevatron, the LHC and a future ILC, J. High Energy Phys. 11 (2014) 039.
[48] P. Bechtle, S. Heinemeyer, T. Klingl, T. Stefaniak, G. Weiglein, and J. Wittbrodt, HiggsSounds-2: Probing new physics with precision Higgs measurements in the LHC 13 TeV era, Eur. Phys. J. C **81**, 145 (2021).
[49] J. Haller, A. Hoecker, R. Kogler, K. Mönig, T. Peiffer, and J. Stelzer, Update of the global electroweak fit and constraints on two-Higgs-doublet models, Eur. Phys. J. C **78**, 675 (2018).
[50] W. Grimus, L. Lavoura, O. M. Ogreid, and P. Osland, The Oblique parameters in multi-Higgs-doublet models, Nucl. Phys. **B801**, 81 (2008).
[51] CDF Collaboration, High-precision measurement of the W boson mass with the CDF II detector, Science **376**, 170 (2022).
[52] Planck Collaboration, Planck 2018 results. VI. Cosmological parameters, Astron. Astrophys. **641**, A6 (2020).
[53] G. Bélanger, F. Boudjema, A. Goudelis, A. Pukhov, and B. Zaldivar, micrOMEGAs 5.0: Freeze-in, Comput. Phys. Commun. **231**, 173 (2018).
[54] LZ Collaboration, First dark matter search results from the LUX-ZEPLIN (LZ) experiment, Phys. Rev. Lett. **131**, 041002 (2023).
[55] T. Biekötter, P. Gabriel, M. O. Olea-Romacho, and R. Santos, Direct detection of pseudo-Nambu-Goldstone dark

matter in a two Higgs doublet plus singlet extension of the SM, J. High Energy Phys. 10 (2022) 126.
[56] M. Muhlleitner, M. O. P. Sampaio, R. Santos, and J. Wittbrodt, The N2HDM under theoretical and experimental scrutiny, J. High Energy Phys. 03 (2017) 094.
[57] I. Engeln, M. Mühlleitner, and J. Wittbrodt, N2HDECAY: Higgs boson decays in the different phases of the N2HDM, Comput. Phys. Commun. **234**, 256 (2019).
[58] F.-A. Fortin, F.-M. De Rainville, M.-A. Gardner, M. Parizeau, and C. Gagné, DEAP: Evolutionary algorithms made easy, J. Mach. Learn. Res. **13**, 2171 (2012).
[59] CMS Collaboration, Search for dilepton resonances from decays of (pseudo)scalar bosons produced in association with a massive vector boson or top quark anti-top quark pair at $\sqrt{s} = 13$ TeV, Technical Report No. CMS-PAS-EXO-21-018, 2022, https://cds.cern.ch/record/2815307.
[60] Fermi-LAT Collaboration, Observations of Milky Way dwarf spheroidal galaxies with the Fermi-LAT detector and constraints on dark matter models, Astrophys. J. **712**, 147 (2010).
[61] Fermi-LAT and DES Collaborations, Searching for dark matter annihilation in recently discovered Milky Way satellites with Fermi-LAT, Astrophys. J. **834**, 110 (2017).
[62] Fermi-LAT Collaboration, The Fermi Galactic Center GeV excess and implications for dark matter, Astrophys. J. **840**, 43 (2017).
[63] D. Hooper and L. Goodenough, Dark matter annihilation in the Galactic Center as seen by the Fermi gamma ray space telescope, Phys. Lett. B **697**, 412 (2011).
[64] T. Daylan, D. P. Finkbeiner, D. Hooper, T. Linden, S. K. N. Portillo, N. L. Rodd, and T. R. Slatyer, The characterization of the gamma-ray signal from the central Milky Way: A case for annihilating dark matter, Phys. Dark Universe **12**, 1 (2016).
[65] T. Biekötter, S. Heinemeyer, J. M. No, K. Radchenko, M. O. O. Romacho, and G. Weiglein, First shot of the smoking gun: Probing the electroweak phase transition in the 2HDM with novel searches for $A \to ZH$ in $\ell^+\ell^- t\bar{t}$ and $\nu\nu b\bar{b}$ final states, arXiv:2309.17431.
[66] ATLAS Collaboration, Search for heavy Higgs bosons decaying into two tau leptons with the ATLAS detector using pp collisions at $\sqrt{s} = 13$ TeV, Phys. Rev. Lett. **125**, 051801 (2020).
[67] P. Drechsel, G. Moortgat-Pick, and G. Weiglein, Prospects for direct searches for light Higgs bosons at the ILC with 250 GeV, Eur. Phys. J. C **80**, 922 (2020).